AJP

ISSN : 0971 - 3093

Vol 28, Nos 10-12, October-December 2019

ASIAN JOURNAL OF PHYSICS

An International Peer Reviewed Research Journal

Advisory Editors : W. Kiefer & FTS Yu

A Special Issue

Dedicated to

Prof Kehar Singh

Formerly Professor of Physics

at IIT Delhi

Guest Editor : R. S. Sirohi

ap

ANITA PUBLICATIONS

FF-43, 1st Floor, Mangal Bazar, Laxmi Nagar, Delhi-110 092, India

B O : 2, Pasha Court, Williamsville, New York-14221-1776, USA

ap

Asian Journal of Physics
Vol. 28, Nos 10-12 (2019) 877-889
Available on: www.asianjournalofphysics.in

Guided wave photonics for light sources, sensors and passive components at mid-IR

Babita Bakshi (nee Kumari)[1], Ajanta Barh[2], Somnath Ghosh[3], Ravendra K Varshney[1] and Bishnu P Pal[4]

[1]*Department of Physic, Indian Institute of Technology Delhi, Dehli-110 016 India*
[2]*Institute for Quantum Electronics, ETH Zürich, CH-8093 Zürich, Switzerland*
[3]*Department of Physics, Indian Institute of Technology, Jodhpur-342 037 Rajasthan, India*
[4]*Mahindra École Centrale, Department of Physics, Hyderabad-500,043, India*

Dedicated to Professor Kehar Singh for his significant contributions to Optics and Photonics

Guided wave photonics has emerged as a versatile mid-infrared (mid-IR) wavelength platform and option for realising light sources, sensors and components in the technologically important wavelength window of 2-25 μm. Portions of this spectral band represent molecular fingerprint regimes of certain molecules' characteristic signature absorption wavelengths, which find extensive applications in pollution detection and bio-chemical-medical research. Mid-IR waveband is also attractive for defense, homeland security, sensing of noxious gases, astronomy, spectroscopy, LIDAR, optical tomography, etc. In this review paper, we present our own research in recent years in the context of highlighting role of guided wave photonics for realizing light sources, sensors, and polarization components for use at mid-IR spectral domain.

Keywords: Optical waveguides, Optical fibers, Nonlinear optics, Four wave mixing, Silicon photonics sensors and components

1 Introduction

Infrared (IR) radiation beyond red light from a prism dispersed pattern of sunlight was discovered, possibly for the first time, by astronomer William Herschel in 1800. In early days near-IR to far-IR spectra were mostly used for passive astronomical applications like detection of terrestrial objects like planets, comets, asteroids etc. In recent years a strong interest has emerged in developing devices capable of operating at wavelengths in the mid-IR range (2-25 μm) in view of their potential applications in areas as wide as astronomy, climatology, civil, medical surgery, military, biological spectroscopy, optical frequency metrology, optical tomography, and sensing [1-5]. More specifically, this wavelength band is technologically important as it encompasses the atmospheric windows like 3-5 μm and 8-14 μm essential for thermal imaging, homing, security e.g. remote detection of explosives, and counter measures against heat-seeking missiles as well as for molecular fingerprints due to strong characteristic vibrational energy transitions bands for absorption of atmospheric and biological molecules [6-9]. It is worth mentioning that many a researcher often refers 2 ~ 10 μm as the mid-IR regime (cf. Fig 1). It is conjectured that since mid-wave infrared (MWIR) of 3-5 μm offers a clear atmospheric window for high power transmission, compact semiconductor and all-fiber light sources should attract applications in defense. The band 3-5 μm is also touted as a potential communication window.

Corresponding author:
e-mail: bishnu.pal@mechyd.ac.in (Bishnu P Pal)

Furthermore, vibration spectra of compounds like As-H, HCHO, CH_3COOH, CH_3, CCl_4, various hydrocarbons, hydrochlorides exhibit strong absorption in the spectral range 5 - 6.5 µm wavelength. In fact, *absorption lines* of protein molecules like amide-I, amide-II and water molecules (H_2O), which are some of the key components of human tissues, fall at 6.1 and 6.45 µm. Hence, this fingerprint wavelength regime is eminently suitable for strong absorption in soft/hard tissue-enabling tissue ablation surgery, e.g., laser surgery for brain, nerve, eye, skin etc. Therefore, it has become strategically important to develop efficient, high power, and compact light source(s) in the mid-IR wavelength domains, which is the topic of discussion in the first part of the present paper. In particular, we focus on designs of all-fiber mid-IR sources based on microstructured specialty optical fiber platform. We exploit the concept of tailored microstructured fiber designs to achieve longer wavelength (mid-IR) source(s) through *wavelength translation* via nonlinear four wave mixing (FWM) process using commercially available high-power laser(s) that operate at near-IR wavelength(s) as the pump(s). Few sample results from our own research would be discussed in the paper.

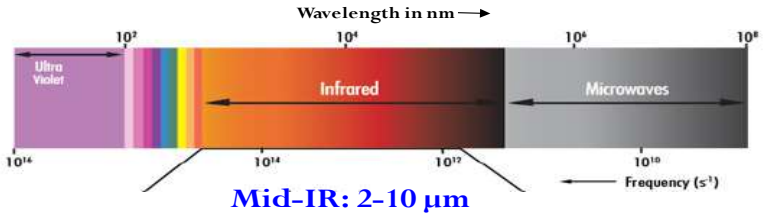

Fig 1. A representative figure for various important regimes of electromagnetic spectrum

In the second part, we would focus on silicon integrated optics for realising certain sensors and polarization components. Miller from the then Bell Laboratories had coined the term Integrated Optics (IO) *fifty years ago* in 1969 in analogy to electronic integrated circuits (IC) [10]. As an example, Miller proposed an IO miniature repeater, which would integrate a photodetector, an amplifier, and a light source on a common substrate much like an IC. In fact, 2019 is being celebrated as 50th anniversary of on-chip optical integration. However, non-availability of a single material to serve as source, detector, amplifier and modulator, drove development along *hybrid technology* route in which different functional units are surface mounted on a common substrate with guided wave components as interconnects between these units. For example, silica on silicon was used as a platform to develop several passive components in 1980s and were summarized in a review article in Progress in Optics [11]. Subsequently a journal special issue devoted to guided wave optics on silicon had also appeared [12]. Primarily driven by applications ranging from social networks and streaming media to genomics-driven medicine and the proliferation of connected devices within the Internet of Things (IoT), an exponential increase in demand for bandwidth (BW) has been seen in recent years so much so that according to UN the number of mobile phone subscribers is already approaching human population on earth! But this increase in data access comes at a cost e.g. a single Internet search consumes about 1 kJ of energy according to Google because these data has to go through a massive monolith of servers and switches. Industry experts had estimated that by 2016 the world's data centers were consuming almost 40% more electricity than what is used by the entire UK. Many of these issues would be substantially mitigated if cables and switches, which provide sever-to-server interconnects were configured to communicate via photons rather than electrons. One potential route to achieve this is silicon photonics, which could enable a chip-scale platform for monolithic integration of optics and microelectronics for applications of optical interconnects in which high data streams are required in a small footprint [13]. Silicon photonics is also sure to find use as a platform for realizing point-of-care bio-photonic healthcare devices [14]. In the second part, we would attempt to briefly describe our own research on designing gas sensors and waveguide components for achieving polarization diversity within the scope of silicon-based Photonic Integrated Circuits (PICs).

2 Fiber for all-fiber mid-IR light source: design methodology and results

It is well known that microstructured optical fibers (MOFs) can be broadly classified into two types, in both of which wavelength scale periodic refractive index features (typically air holes or a material of lower refractive index than the substrate material) form the cladding while the core is formed either with a solid material same as the substrate (i.e. the base material) of size typically larger than the holes (in the cladding) or a hole of bigger size. Former type of MOFs is called index guided MOFs (sometime referred to as holey fiber due to the holes in it) and the latter are called photonic band gap (PBG) fibers. For designing fiber-based devices like sources for mid-IR applications, chalcogenide glasses (S-Se-Te based glass compositions) are promising candidates because of their intrinsic extraordinary linear and nonlinear properties, e.g. lower transmission loss than typical communication fiber made of silica, also the Kerr nonlinearity (nonlinear coefficient n_2) is two orders of magnitude larger than that of silica. Zero dispersion wavelengths (λ_{ZD}) in chalcogenide MOFs can be tailored to fall anywhere between 2 and 11 μm. As is well known [15], during the degenerate FWM process, two pump photons of frequency ω_p get converted into a signal photon ($\omega_s < \omega_p$) and an idler photon ($\omega_i > \omega_p$) according to the energy conservation relation ($2\omega_p = \omega_s + \omega_i$), where subscripts s, i and p stand for signal, idler, and pump, respectively. To study simultaneous evolution of the three waves under quasi-continuous wave (CW) condition, a set of coupled equations are required to be solved simultaneously [15,16] as described in [17]. To achieve maximum frequency shift $\Omega_s = \omega_p - \omega_s = \omega_i - \omega_p$ through the FWM process, phase matching parameter $\Delta\kappa \left[\sum_{m=2,4,6,\ldots}^{\infty} 2\beta_m(\omega_p)\frac{\omega_s^m}{m!}\right]$, where β_m is the m^{th} order group velocity dispersion parameter, should ideally be zero [17]. Considering up to fourth-order dispersion terms, the best route to achieve the phase matching criterion for FWM would be to tailor the total dispersion through fiber design such that λ_{ZD} is very close to the pump wavelength (λ_p) while maintaining a small positive value for β_2 and a large negative value for β_4. We also need to maintain the cutoff wavelength for the first higher order mode as low as possible (below λ_p). By considering an As_2S_3-based holey type MOF geometry (see Fig 2 a) and restricting pump power levels below 5W, we exploited degenerate FWM to generate an all-fiber narrow band (FWHM of 16 nm) light source centered at 4.36 μm through nonlinear wavelength translation by assuming a CW commercially available Tm-doped fiber laser (λ = 2.04 μm), as the pump. Parametric gain of 20.5 dB is attainable that amounted to a power conversion efficiency > 17.6%. Fiber design challenge lies in designing it for λ_{ZD} close to that of the pump; our design yielded λ_{ZD} ~ 2.106 μm. Figure (2 b) shows the generated spectrum [17]. By working with a similar As_2S_3-based index guided MOF with the difference that the holes in the holey cladding were assumed to be filled with borosilicate glass rods, we have shown that mid-IR power levels in excess of 1 W are achievable in the wavelength domain 3.1 - 3.9 μm with amplification factor more than 25 dB by using an Er-doped ZBLAN fiber laser (λ = 2.8 μm) of 5W average power as the pump in a meter-long specialty MOF of our design [18]. A typical result is depicted in Fig (2 c). In [19], by suitably designing an As_2Se_3 based MOF structure with solid core and holey cladding that consisted of 4 rings of hexagonally arranged circular holes filled with polyethersulfone (PES), which substantially induces a lower refractive index contrast between the core and the cladding, we could design all-fiber sources for emission at λ ~ 6 μm via degenerate FWM. Pump was a continuous wave CO laser λ_p 5.6 μm of 5 ~ 10 W power. By tuning the pump wavelength, pump power, fiber dispersion and nonlinear properties, we could demonstrate narrow (N)- and/or broad (B)- band all-fiber light source (λ ~ 6 μm). Parametric amplification > 20 dB is achievable for the N-band source at 6.46 μm with a maximum power conversion efficiency (C_m) ~ 33% while amplification ~ 22 ± 2 dB is achievable for a B-band source over the wavelength range of 5 – 6.3 μm with a C_m > 40% [19]. Figure (2 d) depicts output power from such an all-fiber mid-IR source with wavelength λ.

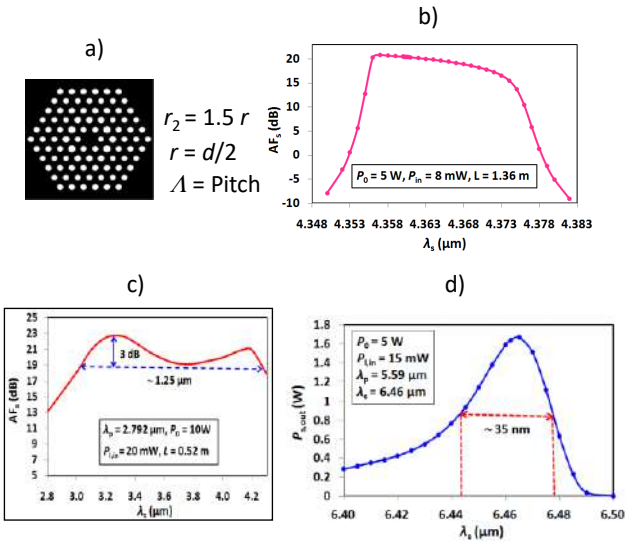

Fig 2.(a) Cross-section of the As_2S_3 MOF in which air-hole diameter of the second ring is r_2 while in rest of the rings it is $r = d/2$, d being the core dimension [17]; (b) generated signal spectrum in terms of amplification factor (AF_s) vs a small power (P_{in}) of idler ($\lambda_i = 1.33$ μm) was also fed into the fiber along with the pump (P_p at 2.04 μm) as the seed 17]; (c) Generated broadband spectrum ($\lambda_s \sim 3.0$ to 4.5 μm) for a similar MOF in which pump was at $\lambda_p = 2.797$ μm and idler seed was ($\lambda_i = 2.19$ μm) [18]; (d) Generated narrow-band spectrum centered at $\lambda_s = 6.46$ μm in a MOF with a CO laser ($\lambda_p = 5.59$ μm) pump and idler ($\lambda_i = 4.94$ μm) [19].

3 Guided wave silicon photonics for on-chip sensors and components

3.1 Introduction to silicon photonics

Silicon (Si) photonics is a versatile complimentary metal oxide semiconductor (CMOS) technology platform that allows integration of nano to micron-scale optical waveguide-based components and sensors with micro-electronics components in a shared Si technology platform and offer attractive features like low footprints due to large refractive index contrast $\Delta n \sim 2.03$ between Si and SiO_2 and ~ 2.48 between Si and Air, which results in strong light confinement and tolerance to very small bend radius ~ 2 μm; low power consumption; holds numerous promises to combine best of both Si ICs and photonic ICs (PICs), - all of which are attractive for large data centers. Typical PICs find applications as delay lines, ring resonators, grating couplers, Mach-Zhender modulators, and directional couplers. Other attractive features of Si in the context of photonics like availability of large wafers, large thermal conductivity ~ 1.3 W cm^{-1} $°C^{-1}$ that enables surface mounting of active components, and its broad transparency window of 1.2 ~ 7 μm can be exploited for configuring sensors in the above-mentioned mid-IR molecular fingerprint regime. Sillicon Photonic biosensors are very promising candidates for achieving truly point-of-care devices for healthcare diagnostics suitable in any place and any time [14]. In this second part of the present review, we would attempt to briefly describe our own recent research on designing gas sensors and waveguide components for achieving polarization diversity within the scope of silicon photonics.

3.2 Silicon slot waveguide-based gas sensors

Optical waveguides in various geometries e.g. channel, ridge, photonic crystal, embedded strip, and slot form the heart of silicon photonics technology [13]. The parameter power confinement factor or evanescent field fraction is defined as

$$\eta \text{ (or } \Gamma) = \frac{\int_{gr} S_z \, dxdy}{\int_{total} S_z \, dxdy} \tag{1}$$

where S_z is -component of the Poynting vector and the lower limit of integration *gr* corresponds to guiding region i.e. the core of the waveguide, and *total* refers to total power carried by a guided mode across entire cross-section of the optical waveguide (OWG). Slot waveguides, which were first proposed in [20], could yield high η. Figure 3 illustrates two versions of slot waveguides: (a) vertical and (b) horizontal [21].

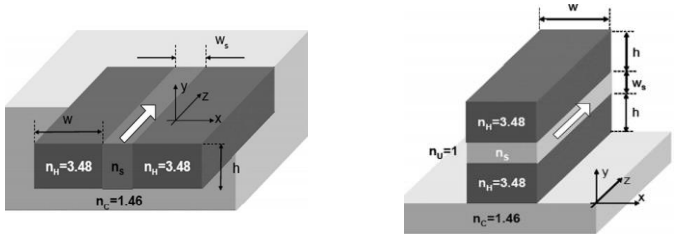

(a) Vertical slot WG (a) Horizontal slot WG

Fig 3. Schematic of (a) vertical and (b) horizontal slot waveguide geometries (after [21]).

Functional principle of slot waveguides rely on the continuity of the normal component of electric displacement vector at the high-index contrast interface between high index Si (H) and low index air in the slot (S), which requires

$$D_S^N = D_H^N \Rightarrow \varepsilon_S E_S^N = \varepsilon_H E_H^N \Rightarrow E_S^N = \frac{n_H^2}{n_S^2} E_H^N \tag{2}$$

where $\varepsilon_{S,H}$ are dielectric permittivity and corresponding refractive indices are $n_{S,H}$ while $D_{S,H}^N$ and $E_{S,H}^N$ represent fields **D** and **E** in the low (i.e. in the slot) and high index regions. From Eq (2), it is obvious that E_S^N in the low index slot is higher than E_H^N in the high index Si by a factor n_H^2/n_S^2 [13]. Ratio $n_H^2/n_S^2 = 6$ for Si/SiO_2 interface and = 12 for Si/air interface. When the slot width ≪ characteristic evanescent field ($E \sim e^{-\gamma_s x}$) decay length ~ $1/\gamma_s$ of the fundamental eigen mode in the slot, **E**-field remains high all across the slot. This fact was exploited in [22, 23] to design trace gas sensors in the mid-IR. In [22], design of a chip-scale evanescent field absorption-based trace NH_3 gas sensor is reported on a silicon-on-nitride (SON of refractive index = 1.9) slot waveguide structure at λ = 3 μm. Figure 4 shows a schematic of the structure and confined field strength η (same as Γ) in the air-filled slot region. Basic physical principle that underlies the sensor is evanescent field of the slot WG mode interacting with the surrounding/exposed gas *induces* significant attenuation (as per Beer-Lamberts law) of the transmitted 3 μm light that corresponds to the absorption line(s) of the gas. Beer-Lamberts Law is given by

$$I = I_0 \, e^{-\Gamma \varepsilon C l - \alpha l} \tag{3}$$

where I_0 is the input light intensity, ε is the absorption coefficient of the sensing gas, α is the intrinsic loss of the waveguide, l is the length of the OWG, and C is the concentration of the sensing gas. Sensitivity of the gas sensor is defined by

$$S = \frac{d(I/I_0)}{dC} = -\Gamma \varepsilon l e^{-\Gamma \varepsilon C l - \alpha l} = -\Gamma \varepsilon l I_{norm} \tag{4}$$

where $I_{norm} = I/I_0$, minus sign is indicator of it being absorptive phenomenon. Sensitivity being proportional to Γ, S can be maximized by enhancing Γ. For the optimum length of the designed OWG l_{opt} = 8.7 mm, I_{norm} as a function of λ is plotted in Fig 5 for three different values of C = 2, 10, 50 ppm and for I_0 = 10 mW.

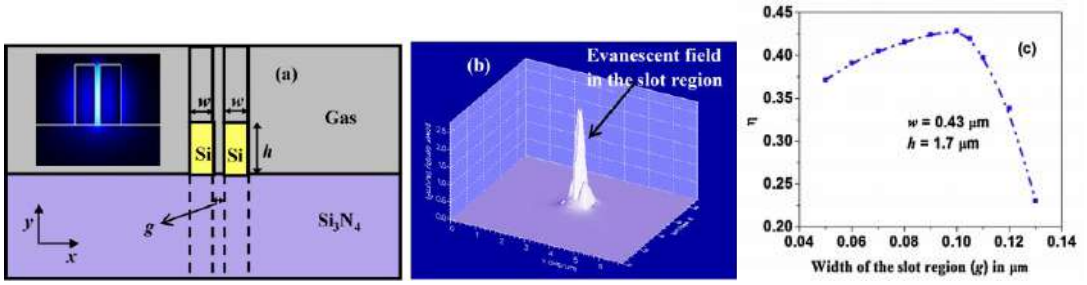

Fig 4.(a) Schematic cross-sectional view of the proposed SON-based slot waveguide and inset shows 2D field distribution of fundamental quasi-TE mode of it; (b) 3D power density profile of the fundamental quasi-TE mode of the proposed slot waveguide structure; (c) mode field confinement as a function of waveguide parameters (adapted from [22]).

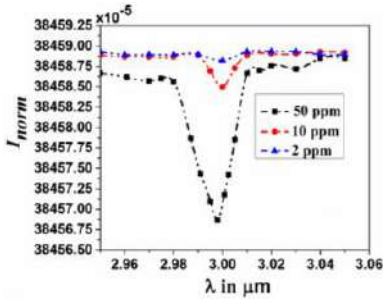

Fig 5. Variation of I_{norm} at the OWG output with λ for three different values of C (2, 10, 50 ppm).

Commercially available quantum cascade laser can be used as the input light source, which offer room temperature operation up to a wavelength of 9 μm along with power level ranging from 10 mW to 100 mW [24]. Mid-IR commercial detectors e.g. PbSe, HgCdTe can be used to detect the output intensity. Minimum resolvable concentration ($C_{\min}$) of a gas is given in Refs [22, 25] as

$$C_{\min} = \frac{NEP}{SI_0 e^{-\alpha l}\sqrt{B}} \tag{5}$$

where NEP is the noise equivalent power and B is the electrical bandwidth of the detector. Using our optimum sensor design, detection of NH_3 gas down to 5 ppm including waveguide loss is viable in just ~ 8.7 mm length of the designed slot waveguide-based gas sensor. Our tolerance studies showed that Γ is relatively more critical to the slot width as compared to its height [22]. Photon Design's FIMMWAVE©: full-vectorial mode solver FMM (film mode matching) was used for obtaining modal characteristics of the slot WG. In [23], by applying same evanescent field absorption sensing scheme, a chip-level silicon rib horizontal double-slot waveguide geometry was proposed and designed for hazardous N_2O trace gas sensing at the mid-IR band regime of 4.47 μm. Designed geometry and sample results are shown in Fig 6. The sensor showed detection down to nearly 0.2 ppm level within 1.44 cm length of our designed waveguide even after including the waveguide losses. With this optimum sensor design, we have also studied detectability of CO and CH_4 gases numerically at the wavelengths of 4.6 μm and, 3.67 μm, respectively, and have shown that minimum detectable concentrations for these gases are nearly 0.44 ppm and 36 ppm, respectively. Table 1 depicts minimum detectable gas concentration ($C_{\min}$) and Γ. Fabrication tolerances of the structure have shown that sensor has high tolerance to fabrication imperfections. It is seen that up to ±10% variations from these optimum WG parameters is tolerable in actual fabrication, because for this kind of variations Γ, still remains > 65%, thereby implying that our design is quite robust for actual fabrication. For maximum sensitivity (S), optimum WG geometric parameters were taken as h = 0.58 μm, h_3 = 0.40 μm, w = 1.05 μm, g = 0.11 μm, r_h

(= h_1/ h) = 0.48, and r_w (= w_1/w) = 0.28 for which Γ was ≈ 69.0%, which is also evident from the contour plot shown in Fig 7; for gap, g ≅ 0.11 µm and h_3 ≅ 0.40 µm, Γ ≈ 0.687 i.e. 68.7%.

Table 1. Values of various parameters for different gases with minimum detectable gas concentration (C_{min}) [23]

Gas	Peak absorption wavelength µm	Γ (%)	Absorption coefficient ε (ppm − cm)$^{-1}$	(ppm) (for SNR = 1)	(ppm) (for SNR = 10)
N_2O	4.47	68	1.075 × 10−4	0.021	0.214
CO	4.6	66.6	5.377 × 10−5	0.044	0.436
CH_4	3.67	65.4	6.721 × 10−7	3.544	36

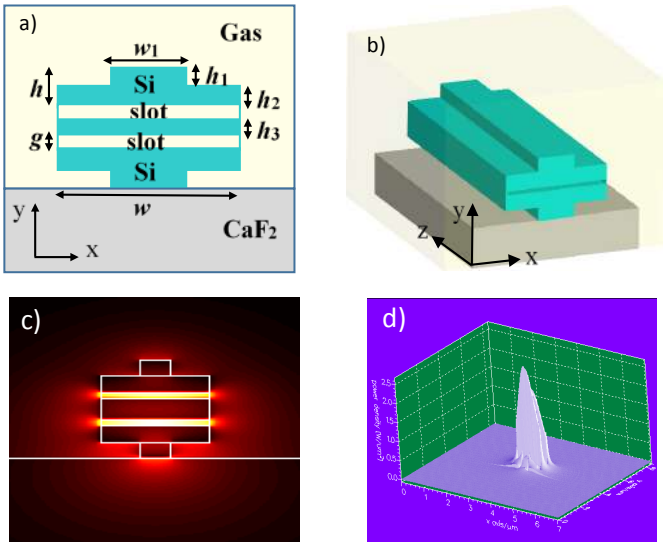

Fig 6. (a) Cross-sectional view of proposed rib horizontal double-slot WG on CaF_2 substrate; (b) 3D view of this WG; (c) 2D field distribution of fundamental quasi-TM mode of the double-slot WG; (d) 3D power density profile of the fundamental quasi-TM mode of this WG (adapted from [23]).

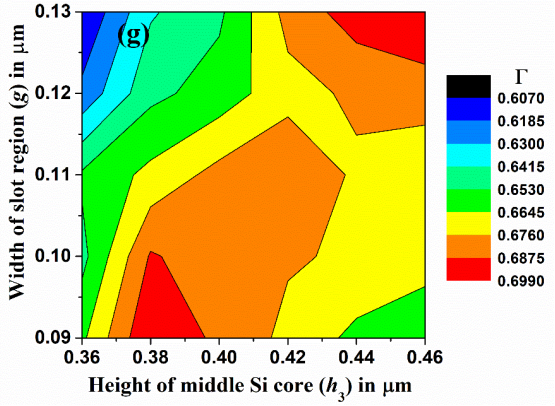

Fig 7. Contour plot of Γ as a function of h_3 and g keeping h = 0.58 µm, w = 1.05 µm, r_h = 0.48, and r_w = 0.28 (adapted from [23]).

3.3 Silicon photonics-based ultra-short Mid-IR polarization splitter

Large refractive index contrast WGs inherently exhibit strong polarization sensitivity in their response. A solution to substantially overcome this strong polarization sensitivity requires deploying a polarization diversity scheme shown in Fig 8 [26]. In [27], we reported an ultra-compact ~ 6.6 µm long polarization splitter (PS) for the mid-IRwavelength of 4.47 µm (N_2O gas absorption line). It is based on a directional coupler made of a horizontal slot waveguide and a strip waveguide with Si as core material and CaF_2 in the slot as well as the substrate material [see Figs 9 (a) and (b)].

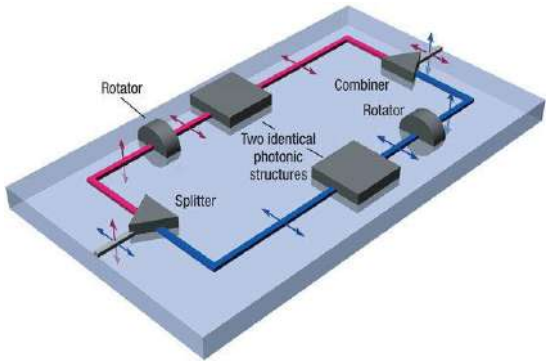

Fig 8. Example of polarization diversity scheme showing use of various components like polarization combiners, rotators, and splitters (adapted from [26]).

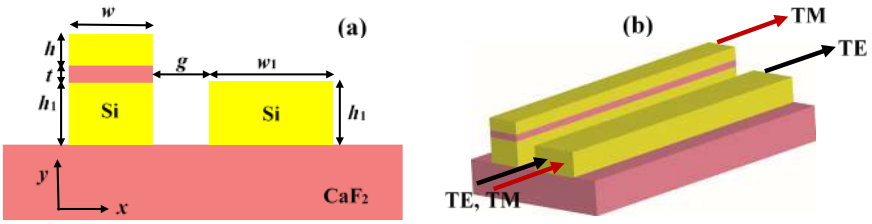

Fig 9. (a) Schematic cross-sectional view of the proposed polarization splitter (PS) and (b) its 3-D view [27].

Eigenmode expansion method by employing software package FIMMPROP©, which was linked with FIMMWAVE© was used to investigate its propagation characteristics. Design was targeted to make the horizontal slot WG support only one quasi-TM mode and the strip WG supports both quasi-TM and quasi-TE modes. Consequently, TM modes of the two WGs will only satisfy the phasematching condition. Accordingly, if the length of the directional coupler is chosen to equal the coupling length (the shortest length required for maximum power transfer) for the TM modes of the two WGs, TM mode of strip WG would get coupled to the slot WG, whereas the TE mode would exit from the throughput port. There are multiple combinations of geometric parameters for TM modes of the two WGs to satisfy the phase matching condition. However, to ensure that confinement of the TM modes is sufficiently high in respective WGs we have chosen $w = 0.58$ µm and that of $w_1 = 0.999$ µm through several iterations. By choosing appropriate additional structural parameters $h = 0.3$ µm, $h_1 = 0.8$ µm, and $t = 40$ nm [27], we have designed the polarization splitter such that only the TM polarization satisfies the phase matching condition for coupling at the targeted wavelength of 4.47 µm. Achieved extinction ratios (ER) were ~ 41.6 dB (with a low insertion loss (IL) of ~ 0.25 dB) and ~ 37.1 dB (with an appreciably low IL of ~ 0.07 dB) for the cross-coupled and the throughput ports, respectively. It can function over a broad bandwidth of 200 nm with high ER (> 37 dB and > 17 dB, for cross-coupled and throughput ports, respectively) and correspondingly low IL (< 0.5 dB and < 0.1 dB, respectively). Figures 10 (a) and (b) depict light propagation along the polarization splitter for TM and TE polarized light, respectively.

It is evident that TM polarized light is cross-coupled after propagating through ~ 6.6 μm while the TE polarized light exits from the throughput port without any cross coupling. TM polarization satisfies the phase matching condition for coupling at the targeted wavelength of 4.47 μm. Achieved extinction ratios were ~ 41.6 dB (with a low insertion loss of ~ 0.25 dB) and ~ 37.1 dB (with an appreciably low IL of ~ 0.07 dB) for the cross-coupled and the throughput ports, respectively. Thus, our design scheme yielded an ultra-short ~ 6.6 μm polarization splitter for the mid-IR wavelength of 4.7 μm.

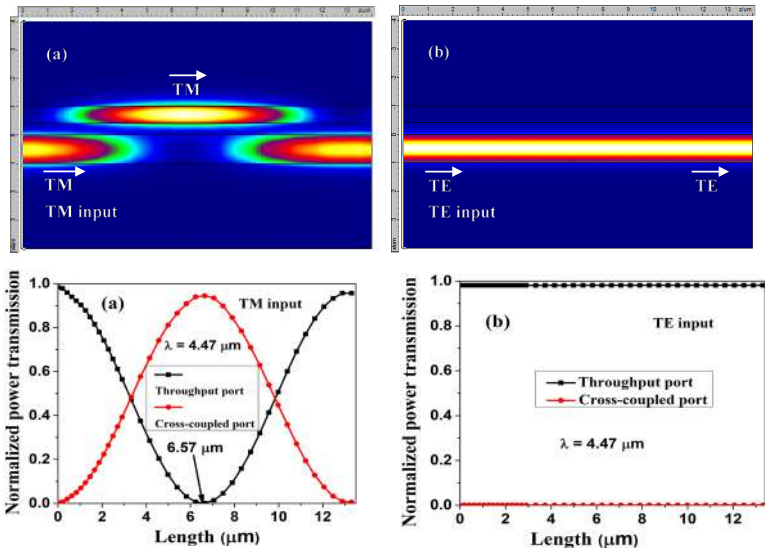

Fig 10. upper figure: intensity variations of TM and TE modes along length of the designed PS (a) when TM is the input and (b) when TE is the input; lower figure: numerically computed normalised power transmission in the two waveguides) as a function of length of the coupler [adapted from [27]).

In order to check the accuracy of our just mentioned approach for designing a PS, we have simulated the results on a experimentally realized PS reported in [28] using two identical horizontal single slot WGs. Results of comparison are shown in Fig 11, in which *ER* for the throughput port is plotted (red dots: experimental results) as a function of length of the fabricated PS [28] alongwith our simulated results (black dots) for the telecommunication wavelength of 1.55 μm. From this figure, it can be observed that our simulated results are in good agreement with the experimental results of PS reported in [28].

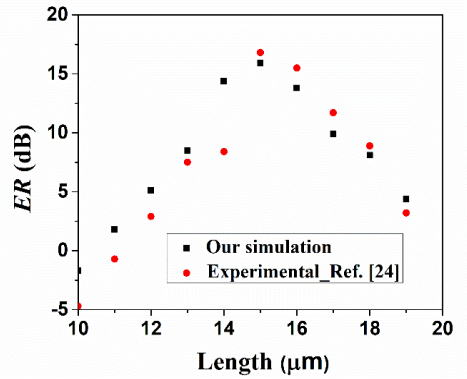

Fig 11. Comparison of our simulation results with the fabricated PS reported in [28] in terms of *ER* for the throughput port (at the wavelength of 1.55 μm) as a function of length of the PS.

3.3 Polarization rotator(PR)

In [29], we have reported design of an efficient polarization rotator. As shown in Fig 12, it is based on an asymmetric directional coupler made of a horizontal slot waveguide and a strip waveguide (WG) on silicon-on-calcium-fluoride platform for the mid-IR regime. In particular, we have optimized it for realizing rotations of both the polarizations at the operating wavelength of 4.47 μm. It is worth noting that silicon-on-calcium-fluoride (SOCF) platform was chosen in place of traditional SOI platform because SiO_2 exhibits high absorption at wavelengths > 3.6 μm [30]. Refractive index of CaF_2 is ~ 1.4 and have low loss transmission windows up to ~ 9 μm, which is a wider transparency window in the mid-IR as compared to other materials such as sapphire (Al_2O_3 of $n \sim 1.7$) and silicon nitride (Si_3N_4 of $n \sim 1.9$) having spectral transparency windows up to ~ 5.5 μm and ~ 7μm, respectively. Power coupling through appropriate phase matching between the quasi-TM mode of the designed horizontal slot WG and the quasi-TE mode of the designed strip WG has been exploited for realizing polarization rotation. Through numerical simulations we have demonstrated that achievable maximum power coupling efficiency (C_m) is as high as ~ 95% (within a device length of ~ 0.57 mm).We have also investigated and optimized in a similar manner a double-slot WG-based structure depicted in Fig 13 and results are presented in Figs 14 and 15. For the double-slot WG geometry, C_m was even better ~ 97% with an even shorter device length of ~ 0.47 mm. Both the designed polarization rotators (PRs) exhibited relatively large bandwidth of 50 nm. Their fabrication should be relatively easy as it would not require etching of nano-sized vertical slot and any kind of tapering. Furthermore, it can convert/rotate an input quasi-TM polarization in the slot WG to a quasi-TE polarization output from the strip WG, and a quasi-TE polarization input in the strip WG to a quasi-TM polarization output from the slot WG with very high-power coupling efficiency of ~ 95%.

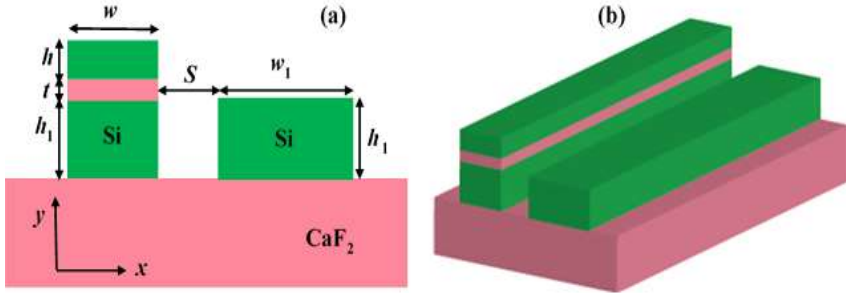

Fig 12. (a) Cross-sectional schematic of the single-slot PR, (b) its 3D view (adapted from [28]).

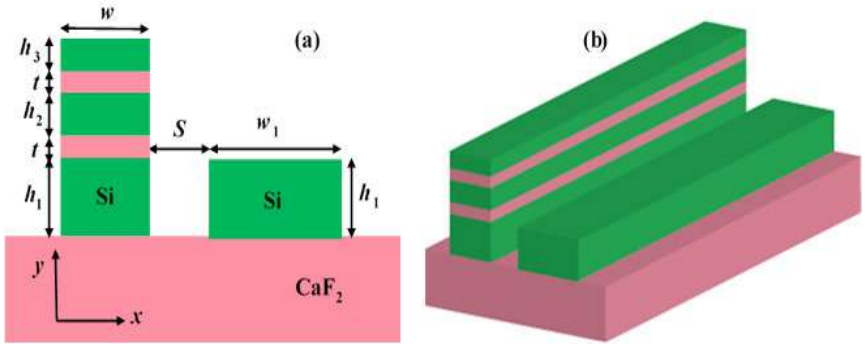

Fig 13. (a) Schematic cross-sectional view of the proposed PR based on double-slot WG geometry, (b) its 3D view (adapted from [29]).

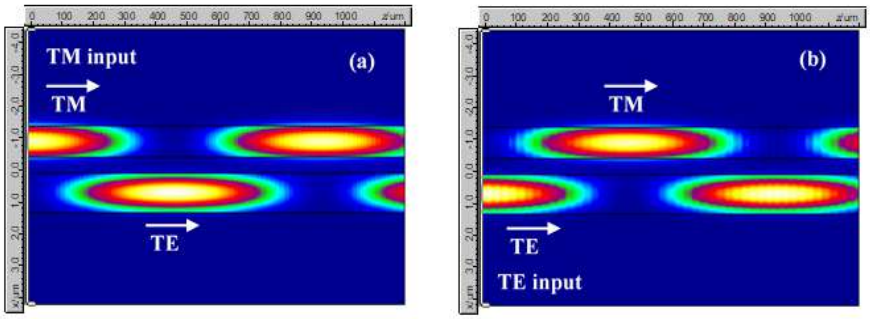

Fig 14. Light propagation in the designed double-slot WG PR with TM mode in the slot WG and TE mode in the strip WG for the cases (a) when TM is input in the slot WG, (b) when TE is input in the strip WG. Here, $w = 0.95$ µm, $w_1 = 1.221$ µm, $h_1 = 0.8$ µm, $h_2 = 0.35$ µm, $h_3 = 0.05$ µm, and $t = 0.02$ µm (adapted from [29]).

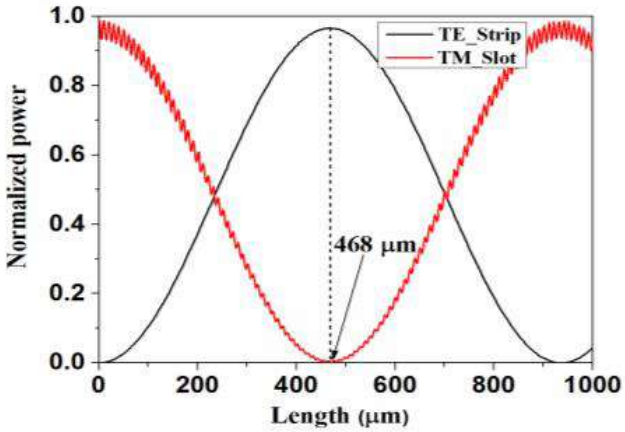

Fig 15. The normalized power variations of TE mode in the strip WG (black curve) and TM mode in the slot WG (red curve) as a function of the device length for the double-slot PR (adapted from [29]).

4 Conclusions

In this paper, we have presented a review of our recent research on the role of guided wave mid-IR photonics to realise all-fiber sources, silicon waveguide-based gas sensors, and optical components important for attaining polarization diversity. Several sample results are presented for guided wave mid-IR light sources, noxious gas sensors through silicon slot waveguides, and polarization components like polarization splitter and polarization rotator for mid-IR wavelength by exploiting strong mode power confinement in Si slot waveguides in the context of deploying polarization diversity in silicon photonic integrated circuits.

Acknowledgement

One of the authors BPP thanks Guest Editor, Prof R S Sirohi for his invite to contribute to this special issue dedicated to significant contributions in optics and photonics made by Professor Kehar Singh, BPP and RKV's erstwhile long-time colleague at IIT Delhi and wishes to gratefully acknowledge many stimulating discussions on a variety of topics and for his motivation and belief that a lot is achievable in science when pursued with sincere and conscientious hard work.

References

1. Sanghera J S, Aggarwal I D, Active and passive chalcogenide glass optical fibers for IR applications: a review, *J Non-Cryst Solids*, 256-257(1999)6-16.
2. Rolfe P, *In-vivo* near infrared spectroscopy, *Annu Rev Biomed Eng*, 2(2000)715-754.
3. Serebryakov V A, Boĭko É V, Petrishchev N N, Yan A V, Medical applications of mid-IR lasers, problems and prospects, *J Opt Technol*, 7(2010)6-17.
4. Hartl I, Li X D, Chudoba C, Ghanta R K, Ko T H, Fujimoto J G, Ranka J K, Windeler R S, Ultra-high-resolution coherence tomography using continuum generation in an air-silica microstructured optical fiber, *Opt Lett*, 26(2001)608-610.
5. Jackson S D, Towards high power mid-infrared emission from a fibre laser, *Nat Photonics*, 6(2012)423-431.
6. Pile D, Horiuchi N, Won R, Graydon O, Extending opportunities, *Nat Photonics,* 6(2012)407; doi:10.1038/nphoton.2012.149
7. Soref R A, Emelett S J, Buchwald W R, Silicon waveguided components for the long-wave infrared region, *J Opt A*: *Pure and Appl Opt*, 8(2006)840-848.
8. Hu J, Meyer J, Richardson K, Shah L, Feature issue introduction: mid-IR photonic materials, *Opt Mater Exp*, 3(2013)1571-1575. :
9. Lin H, Luo Z, Gu T, Kimerling L C, Wada, Agarwal A, Hu J, Mid-infrared integrated photonics on Silicon: a perspective, *Nanophotonics*, 7(2018)393-420.
10. Miller S E, Integrated optics: an introduction, *Bell Syst Tech J*, 48(1969)2059-2069.
11. Pal B P, Guided wave optics on silicon: Physics, technology and status, Chapter 1 in *Progress in Optics,* Wolf E (ed), vol. XXXII(Elsevier Science Publishers B.V.),1993, pp 1-59.
12. Pal B P, Syms R R A (Guest Editors), Special issue on guided-wave optics on silicon, IEE Proc. Optoelectron, 143 (1996).
13. Lipson M, Guiding, modulating, and emitting light on silicon-challenges and opportunities, *J Lightwave Technol*, 23(2005)4222-4228.
14. Gonzalez-Guerrero A B, Dante S, Duval D, Osmond J, Lechuga L M, Advanced photonic biosensors for point-of-care diagnostics, *Procedia Engg*, 25(2011)71-75.
15. Agrawal G P, *Nonlinear Fiber Optics* 4th edn, (Academic Press, San Diego, CA), 2007.
16. Cappellini G, Trillo S, Third-order three wave mixing in single-mode fibers: exact solutions and spatial instability effects, *J Opt Soc Am B*, 8(1991)824-838.
17. Barh A, Ghosh S, Agrawal G P, Varshney R K, Aggarwal I D, Pal B P, Design of an efficient mid-IR light source using chalcogenide holey fibers: A numerical study, *J Opt.* 15(2013)035205 (4 pages); doi:10.1088/2040-8978/15/3/035205
18. Barh A, Ghosh S, Varshney R K, Pal B P, An efficient broad-band mid-wave IR fiber optic light source: design and performance simulation, *Opt Exp*, 21(2013)9547-9555.
19. Barh A, Ghosh S, Varshney R K, Pal B P, Sanghera J, Shaw L B, Aggarwal I D, Mid-IR fiber optic light source around 6 μm through parametric wavelength translation, *Laser Phys*. 24(2014)115401 (7 pages); doi.org/10.1088/1054-660X/24/11/115401
20. Almeida V R, Xu Q, Barrios C A, Lipson M L, Guiding and confining light in void nanostructure, *Opt Letts*, 29(2004)1209-1211.
21. Sanchis P, Blasco J, Martínez A, Marti J, Design of silicon-based slot waveguide Configurations for optimum nonlinear performance, *J Lightwave Tech*, 25(2007)1298-1305.
22. Kumari B, Barh A, Varshney R K, Pal B P, Silicon-on-nitride slot waveguide: A promising platform as mid-IR trace gas sensor, *Sensors and Actuators* B, 236(2016)759-764.
23. Kumari B, Varshney R K, Pal B P, Design of chip-scale silicon slot waveguide for sub-ppm detection of N_2O gas at mid-IR band, *Sensors and Actuators* B, 255(2016)3409-3416.
24. Jones T B, Spott A, Ilic R, Spott A, Penkov B, Asher W, Hochberg M, Silicon-on-sapphire integrated waveguides for the mid-infrared, *Opt Exp*, 18(2010)12127-12135.

25. Huang Y, Kalyoncu S K, Song Q, Boyraz O, Silicon-on-sapphire waveguides design for mid-IR evanescent field absorption gas sensors, Conference on Lasers and Electro-Optics (CLEO) Tech Digest OSA, 2012, Paper JW2A, 122(2012)1-2.
26. Barwitcz T, Watts M R, Popovic M A, Rakich P T, Socci L, Kärtner F X, Ippen E P, Smith H I, Polarization-transparent microphotonic devices in the strong confinement limit, *Nature Photon,* 1(2007)57-60.
27. Kumari B, Varshney R K, Pal B P, Design of a silicon-on-calcium-fluoride-based ultra-compact and highly efficient polarization splitter for the mid-IR, *Opt Eng*, 58(2019)037102, 9 pages; doi: 10.1117/1.OE.58.3.037102
28. Zhang H, Huang Y, Das S, Li C, Yu M, Lo P G Q, Hong M, Thong J, Polarization splitter using horizontal slot waveguide, *Opt Exp*, 21(2013)3363-3368.
29. Kumari B, Varshney R K, Pal B P, Design of a silicon-on-calcium-fluoride-based compact and efficient polarization rotator for the mid-IR, *OSA Continuum* 1(2018)1158-1171.
30. Nedeljkovic M, Khokhar A Z, Hu Y, Chen X, Penades J S, Stankovic S, Chong H M H, Thomson D J, Gardes F Y, Reed G T, Mashanovich G Z,Silicon photonic devices and platforms for the mid-infrared, *Opt Mater Exp*, 3(2013)1205-1214.

[*Received*: 13.10.2019; *accepted:* 23.10.2019]

Babita Bakshi (nee Kumari) is a PhD student in the Department of Physics of Indian Institute of Technology Delhi, India since July 2013. She received her MTech degree from Indian Institute of Technology Kharagpur, India in Solid State Technology in May, 2013. She is a student member of OSA and SPIE. She received the Best Student Paper award at IEEE Workshop on Recent advances in Photonics (WRAP 2017) held at MEC Hyderabad in December 2017. Her research interests include polarization splitters/rotators, guided wave optical sensors, and silicon photonics.

Ajanta Barh received the MSc and PhD degrees in Physics from Indian Institute of Technology Delhi, New Delhi, India, in 2010 and 2015, respectively. In 2016, she joined Optical Sensor Technology group at DTU Fotonik, Technical University of Denmark as a postdoc, where she developed frequency upconversion based broadband optical detection systems for mid-infrared sensing and imaging. In 2019, she joined the Ultrafast Laser Physics group at ETH Zurich, Department of Physics, as a senior postdoc. Currently she is working on ultrafast solid state and semiconductor laser systems operating in the mid-infrared, towards application in frequency metrology and sensing. Ajanta has authored/co-authored more than 50 peer-reviewed journal and conference publications. Her current research interests include mid-infrared photonics, nonlinear optics, upconversion detection, ultrafast laser development and application. She is a young professional member of OSA, and currently chairing the OSA-Nonlinear Optics Technical group.

Dr. Somnath Ghosh, is currently an Assistant Professor in Indian Institute of Technology Jodhpur, Rajasthan, India. He is also the Associate Dean (Academics PG) at IIT Jodhpur from 2018 onward. He has been working in photonics over

10 years and his research work revolves around the domain of photonics which exclusively includes behavioural study of light through random disordered lattices, specialty optical fibers and certain unconventional photonic devices that holds hidden singularities within. To date, he has a total of 106 publications including international journals, conferences, international and national workshops and several invited talks. He is also reviewer of 27 reputed international journals namely Scientific Reports (Nature), Optics Express (USA), Optics Letters, IEEE Photonics Journal and many more.

Earlier, Dr. Ghosh completed his Bachelor in Science from University of Calcutta in Physics. He obtained his Master in Science from Indian Institute of Technology Kharagpur (IITKGP) in Physics with specialization in Optics and Photonics. Later, he joined IITD to pursue his Ph D in Photonics. During his Ph D, he has obtained a number of best research paper awards for his excellent work. Also, he had visited Heriot-Watt University and City University, London as a Visiting Researcher from 2008 to 2010. In 2013, he was awarded as INSPIRE Faculty by Indian National Science Academy and DST, India. He is also a former faculty of Institute of Radio Physics and Electronics, University of Calcutta.

R. K. Varshney received M.Sc. (from Agra University, India) and Ph.D. (from Indian Institute of Technology Delhi, India) in 1981 and 1987, respectively. Presently he is Professor of Physics at IIT Delhi. He is a recipient of Fulbright and Marie Curie Fellowships. He was visiting scientist at various universities such as University of Florida (USA), University of Strathclyde (UK), University of Twente (The Netherlands), University of Nice (France), University of Jean Monnet (France). He is the coauthor of two books ("Fiber Optica" and "Electromagnetics, Problems and Solutions", with Prof. A.K. Ghatak, Prof. I. C. Goyal and Prof. K. Thyagarajan). He has published more than 150 research papers in reputed international journals and conferences. His current research interest is in the field of specialty optical fibers, silicon photonics, mid-IR photonics, THz photonics, fiber optic sensors, and Nonlinear Optics. He is a Fellow of the Optical Society of India and Member of the Optical Society OSA.

Bishnu P. Pal is currently Professor of Physics and Dean of Academics at Mahindra École Centrale at Hyderabad India. He has been Former Chair of Physics Department (2007-2011) and Computer Services Centre both at IIT Delhi (2003-2006) India, Member Board of Directors of OSA The Optical Society (Washington, USA, 2009-2011), Fellow of OSA the Optical Society (USA) and SPIE The International Society for Optics and Photonics (USA), Distinguished Honorary Member of Royal Norwegian Academy of Sciences and Letters (DKNVS, Norway), Senior Member of IEEE (USA) and Distinguished Lecturer of IEEE Photonics Society (2005-2006), Distinguished Life Fellow and President of Optical Society of India (2012-March 2015), Alexander von Humboldt Fellow (1982-83, Germany) at Fraunhofer IPM Freiburg and Fulbright Scholar at NIST Boulder CO (1991, USA), PDF and latter Visiting Professor of Royal Norwegian CSIR (NTNF, Oslo, 1975-77) at Norwegian University of Science and Technology Trondheim Norway, awardee of Esther Hoffman Beller Medal of OSA The Optical Society (Centenary Year 2016, USA), Invited faculty at the ICO Winter School in Optics held at ICTP 1998, Awardee of Homi Bhabha award in Applied Physics of UGC (India, 2006), Om Prakash Bhasin award in Electronics and Information Technology (India, 2013), Khosla Research Award of IIT Roorkee (India, 2014) for lifetime contributions in research, Prof Y T Thathachari award for excellence in Physical Sciences (India, 2010) of Brhamara Trust (Mysore), CEOT award of IETE (India, 2010) for his contributions to Optoelectronics Devices, Co-recipient of the Fiber Optics Person of the Year award (1997) established by Lucent Technology in India and Optics award of Optical Society of India (OSI, 2010) for lifetime achievements.